Exp Fluids (2013) 54:1426
DOI 10.1007/s00348-012-1426-x

RESEARCH ARTICLE

Time-resolved OCT-μPIV: a new microscopic PIV technique for noninvasive depth-resolved pulsatile flow profile acquisition

Chia-Yuan Chen · Prahlad G. Menon · William Kowalski · Kerem Pekkan

Received: 30 May 2012 / Revised: 19 November 2012 / Accepted: 7 December 2012 / Published online: 30 December 2012

Abstract In vivo acquisition of endothelial wall shear stress requires instantaneous depth-resolved whole-field pulsatile flow profile measurements in microcirculation. High-accuracy, quantitative and *non-invasive* velocimetry techniques are essential for emerging real-time mechano-genomic investigations. To address these research needs, a novel biological flow quantification technique, OCT-μPIV, was developed utilizing high-speed optical coherence tomography (OCT) integrated with microscopic Particle Image Velocimetry (μPIV). This technique offers the unique advantage of simultaneously acquiring blood flow profiles and vessel anatomy along arbitrarily oriented sagittal planes. The process is instantaneous and enables real-time 3D flow reconstruction without the need for computationally intensive image processing compared to state-of-the-art velocimetry techniques. To evaluate the line-scanning direction and speed, four sets of parametric synthetic OCT-μPIV data were generated using an in-house code. Based on this investigation, an in vitro experiment was designed at the fastest scan speed while preserving the region of interest providing the depth-resolved velocity profiles spanning across the width of a micro-fabricated channel. High-agreement with the analytical flow profiles was achieved for different flow rates and seed particle types and sizes. Finally, by employing blood cells as non-invasive seeding particles, in vivo embryonic vascular velocity profiles in multiple vessels were measured in the early chick embryo. The pulsatile flow frequency and peak velocity measurements were also acquired with OCT-μPIV, which agreed well with previous reported values. These results demonstrate the potential utility of this technique to conduct practical microfluidic and non-invasive in vivo studies for embryonic blood flows.

C.-Y. Chen
Department of Mechanical Engineering, National Taiwan University of Science and Technology, Taipei 10607, Taiwan

P. G. Menon · W. Kowalski · K. Pekkan
Departments of Biomedical and Mechanical Engineering, Carnegie Mellon University, 700 Technology Drive, Pittsburgh, PA 15219, USA

K. Pekkan (✉)
Department of Mechanical Engineering, Koc University, Rumelifeneri, Istanbul, Turkey
e-mail: kpekkan@andrew.cmu.edu; kpekkan@ku.edu.tr

1 Introduction

Three-dimensional (3D) quantitative hemodynamic analysis is critical for understanding cardiovascular biology associated with mechanosensitive molecular signaling pathways (Roman and Pekkan 2012). In addition to the several mechanical loading theories, widely accepted mechanisms for mechanotransduction include the elongation of endothelial basal membrane and the deflection of the endothelial cilia or glycocalyx due to flow-induced wall shear stress (WSS) (Hove et al. 2003; Weinbaum et al. 2007; Hahn and Schwartz 2009). An accurate non-invasive micro-flow measurement technique with whole-field imaging acquisition capability, that will complement the existing measurement protocols, is necessary for quantitative non-invasive assessment of cardiac function and wall shear stress (WSS).

Two-dimensional (2D) micro-particle image velocimetry (μPIV) (Lee et al. 2007; Poelma et al. 2008) is an established in vivo technique, but limited in depth resolution for accurate WSS estimation. As a remedy, the confocal-μPIV techniques are introduced to provide extremely high near wall resolution, as demonstrated by Park et al. (2004)

and our recent study (Patrick et al. 2011). These techniques were further applied with 3D in vivo data where velocity profiles were acquired through challenging embryonic aortic arch vessels (Corti et al. 2011; Chen et al. 2011). Still, for normal Hematocrit blood with almost no light transmission, the utilization of confocal-μPIV technique is not feasible at depths greater than ~35 μm. This challenge holds even in two-photon mode with long-working-distance objectives, due to the high-energy absorption of Hemoglobin (data not shown). A 3D micro-technique that utilizes deconvolution microscopy (Park and Kihm 2006) is proposed but there is still a need for a new imaging technique with greater depth resolution (~1mm) that exceeds the performance of confocal-μPIV. Measurement performance ranges of contemporary μPIV techniques for high hematocrit blood measurements are summarized in Table 1.

Over the last decade, non-invasive velocity field acquisition (that do not require external particle tracers) has advanced significantly. A well-known example is the X-ray PIV that was developed to study high hematocrit blood flow (Kim and Lee 2006). Likewise, the 3D magnetic resonance (MR)-velocity mapping (also known as phase-contrast-MRI, PC-MRI), employed widely to assess both vascular anatomy and flow in 3D (Markl et al. 2007). Although PC-MRI can now provide volumetric resolution that is close to computational fluid dynamics simulations in three-velocity components (Sundareswaran et al. 2011), it has limited temporal resolution. PC-MRI requires significant computational resources for image reconstruction (Frakes et al. 2008) and signal analysis to reduce artifacts (Bogren et al. 2004; Markl et al. 2007). The spectral Doppler optical coherence tomography (SD-OCT) technique employs the same principle as the PC-MRI, by utilizing IR-light and measuring the Doppler frequency shifts caused by fluid flow. This technique does not require intensive image pre-processing and has been applied to in vivo microcirculation experiments for hemodynamic assessments (Davis et al. 2009). In summary, both PC-MRI and SD-OCT techniques are *imaging modalities*, and unlike PIV, they cannot be regarded *a gold-standard* for quantitative flow measurement.

Table 1 Optical data of various μPIV techniques for high Hct (>10 %) flow measurements

PIV method	Depth resolution	Max. imaging depth
Stereo μPIV	10^1 μm[a]	10^1 μm[a]
Confocal-μPIV	10^1 μm[b]	10^1 μm[c]
OCT-μPIV	10^1 μm[d]	10^1 μm[d]

[a] Data were acquired using the same optical set-up and objective as described in Lindken et al. (2006)

[b] Patrick et al. (2011), Lima et al. (2006)

[c] Patrick et al. (2011)

[d] Davis et al. (2009)

In addition to the PC-MRI and SD-OCT, ultrasound-based techniques are also widely utilized in clinical applications involving large arteries (Weissmann-Brenner et al. 2012). For instance, at the millimeter scale, high-resolution pulsed-Doppler ultrasound microscopy is proved to be useful (Oosterbaan et al. 2009) for flow field assessment in avian embryos and provided detail in vivo micro-scale time-resolved intracardiac velocity waveforms in mouse embryos (Srinivasan et al. 1998). However, ultrasound velocimetry techniques are limited by the Doppler effect to velocities parallel to the ultrasound beam (Zheng et al. 2006) resulting in uncertainty due to 3D vessel orientation. Small ultrasound probes have high center frequency (50 and 40 MHz) reaching 30–40 μm axial resolution and 9–15 mm depth to provide 2-dimensional images (B-Mode), as well as flow direction change during the cardiac cycle (M-Mode), blood flow velocity patterns (pulsed-Doppler, PD), and flow direction (color-Doppler). The high-resolution ultrasound has significantly better spatial imaging resolution and much greater pulsed-Doppler velocimetry recording accuracy than routine clinical ultrasound systems. Employing flow-tracers to augment the ultrasound signal led to the development of an Echo-PIV technique (Kim et al. 2004). Specifically, digital B-mode images of contrast agent particles are used and the velocities of the ultrasound-imaged particles are determined using PIV analysis.

In vivo hemodynamic analyses require high temporal resolution to capture the details of the dynamic blood flow kinematics in microcirculation for accurate estimation of instantaneous WSS. Among all state-of-the-art imaging techniques as introduced in the previous paragraphs, the confocal microscopy is no doubt the most accurate imaging tool but with relative low scanning rate compared to other methodologies. To author's knowledge, the maximum frame rate of a confocal microscope can reach to 420 fps if the image size is shrunk (512 × 16 pixels). On the contrary, a micro-doppler velocimetry tool can record images at a higher rate of 740 fps when the field of view (FOV) is 4 mm × 4 mm. While the OCT system can further be operated at 500 kHz for data acquisition for a FOV of 5 mm × 3 mm. Considering only the accurate WSS estimation, although the confocal microscopy can provide the best resolution both blood cells and vessel walls need to be fluorescently labeled. On the other hand, OCT imaging becomes extremely advantageous since no fluorescent labeling is needed.

In this manuscript, a practical micro-scale and high-speed (>80 Hz) velocity field acquisition technique that combines μPIV analysis and time-resolved OCT image acquisition is introduced for the first-time in the literature.

Analogous to the echo-PIV technique but more suitable for microscopic pulsatile flows, OCT-μPIV technique is also non-invasive as it can employ red blood cells as particles. Unlike SD-OCT (Davis et al. 2009), OCT-μPIV does not require the high-cost volumetric image acquisition to find the angle of the vessel orientation for post-processing of the recorded in vivo data. The new OCT-μPIV technique was first validated using data from extensive synthetic (simulated) PIV data sets and in vitro microchannel experiments. This know-how allowed us to appropriately sample the in vivo *time-resolved* volumetric velocity profiles from embryonic avian microcirculation. Due to its depth-resolved, angle-of-orientation–independent measurement capabilities and relatively low hardware cost, OCT-μPIV found to be a practical technique for both in vivo and micro-fluidic studies.

Organization of this manuscript is as follows. Experimental methodology applied in this work is presented in Sect. 2. Synthetic PIV data sets were first generated and discussed in the Sect. 3 using a parametric in-house code accepting a multitude of realistic input parameters to evaluate the effects of OCT scan direction and scan speed on μPIV results. In addition to the OCT scan specifications, these synthetic test cases were designed to mimic the particle movement and flow conditions observed under physiological conditions of blood flow in chick embryos. To demonstrate accuracy, the depth-resolved particle flow profiles acquired across the width of a microchannel are compared with the corresponding analytical solutions. Following this in vitro test, an in vivo test campaign was performed where time-dependent pulsatile flow profile was quantified in an arterial blood vessel of early chick embryo. These test cases progress logically along with pertinent discussion and comparison to previous studies. Finally, in the Sect. 4, the utility of this work is summarized.

2 Materials and methods

2.1 Evaluation of the scan direction and speed using *synthetic* OCT-μPIV data

To test scanning associated image artifacts, four sets of time-lapse synthetic data sets were generated using an in-house particle generator and flow-simulator, written in Matlab (The MathWorks, Inc., MA) where main scan parameters can be altered. Time-lapse depth-resolved 2D OCT B-mode (depth vs. lateral position) images were assembled from A-scan (a single line of data through the depth, 759-pixel) during each acquisition time instant, which is different from standard whole-field PIV capture. The image size of each time-lapse synthetic frame was 380 × 192-pixel (width × depth, 1 × 0.5 mm^2) with 30,303 μs of equal time difference between any two consecutive frames. Distribution of tracer particles in each synthetic frame was generated from a Gaussian normal distribution function. The intensity of each particle in the image was determined randomly in time and space from a normal error distribution. Flow velocities of these four data sets were matched to the microchannel validation tests and were at the same order as the in vivo chick embryo circulation employed later in this study (Sect. 3.3). Specifically, tracer particle displacement was simulated by fitting to a Poiseuille flow profile with 1 mm/s of peak velocity. The displacement of tracer particles was computed to be 11.5 pixels in the center of image and reduced gradually toward both side walls and was zero on the walls.

To estimate the error caused by different scan directions at different scan speeds, the first test data set was simulated using a traditional whole-field PIV CCD capture method with a frame rate of 380 fps. In the second test case, all test conditions were the same as the first one except the scan speed was simulated to be 33 fps and the scan direction was parallel to the main flow direction, which is the same as the in vivo test. In the third test case, all conditions and scan procedure were repeated with the only change of the scan rate increased to 80 fps. Fourth case and the fifth test cases are similar to the second and third test cases, respectively, with the only change of scan direction from parallel to perpendicular, to the main flows direction. Throughout these parametric tests, as summarized in Table 2, the artifacts caused by the scan speed and direction were quantified to serve as a baseline to determine the optimal parameters for conducting OCT-μPIV in vivo and for possible micro-fluidic applications.

2.2 Fabrication of microchannels and experimental set-up

Deep polydimethylsiloxane (PDMS) microchannels with 400 μm wide, 780 μm high were fabricated using a double-coating photolithography process to make a thick SU-8 mold (Patrick et al. 2011), followed by PDMS casting and

Table 2 Synthetic data test matrix of parametric cases for the new OCT-μPIV technique

Test case	Scan direction	Scan speed
1	CCD capture	NA
2	Parallel to the flow direction	33 fps
3	Parallel to the flow direction	80 fps
4	Perpendicular to the flow direction	33 fps
5	Perpendicular to the flow direction	80 fps

These synthetic PIV images were used to evaluate the effect of scan speed and its direction. CCD capture corresponds to the traditional instantaneous whole-field PIV acquisition

finally bound to a cover slip (No. 1, 0.15 mm) through oxygen plasma bombardment. The rectangular geometry of the PDMS mold was confirmed by optical microscopy with calibrated scale. Polyethylene tubing (Braintree Sci., MA) was connected to the inlet and outlet of the microchannel. A calibrated pulsatile syringe pump (Harvard Apparatus, MA) was selected to provide pressure driven flows at 10.6, 21.1, and 31.1 μl/min. 3.2 μm diameter florescent polystyrene particles (Microgenics, Inc., CA) were added to the working fluid (distilled water) so that the flow fields could be studied. Experiments were performed with a range of PIV particles in order to determine the optimal particle type and size, which are summarized in "Appendix".

2.3 Optical coherence tomography

The principles and design of OCT have been described in detail elsewhere (Huang et al. 1991; Brezinski 2006; Drexler and Fujimoto 2008). Relevant properties of the OCT probe used in this study (Ganymede, Thorlabs, Inc., NJ) are briefly discussed. OCT uses low-coherence interferometry to measure the axial distance of back-reflected light, producing a 2D B-scan similar to echo-based modalities such as ultrasound (Huang et al. 1991). Interferometry detects interference fringes that occur when two beams split from a single light source are recombined (Brezinski 2006). If the light source is temporally coherent, then differences in the paths of the two beams (path length, refractive index, etc.) will create a phase shift, which can be measured from the fringe pattern (Brezinski 2006). A light source with a short coherence time, however, will only generate a fringe pattern if the path lengths of the beams are the same. In OCT, low-coherence light is split into a reference arm that travels over a known path length, and a sample arm, which travels through the structure of interest. When passing through biological tissue, changes in index of refraction due to tissue heterogeneity produce reflections, which are returned along the sample arm. When the reference and sample arms are combined, only back-scattered reflections from a depth in the tissue equal to the length of the reference arm produce interference fringes. Performing a scan for various reference arm lengths generates a single A-line showing back-scattered intensity versus axial depth; this formulation is time-domain OCT (Drexler and Fujimoto 2008). The spectral domain (SD) system used in this study does not require movement of the reference arm to generate the A-line. Instead, the combined reference and sample arms are sent to a spectrometer consisting of a diffraction grating and line-scanning CCD camera to create a spectral interferogram (Brezinski 2006). A Fourier transform can then be used to calculate the A-line. This form of OCT allows faster scan rates necessary for time-resolved investigations.

The OCT system used in this study employs a 930-nm center wavelength superluminescent diode with a spectral bandwidth (FWHM) of 100 nm as its light source. The 930-nm source is ideal for OCT as, given the absorptive and scattering properties of tissues, a "therapeutic window" for optical radiation is 600–1,300 nm (Parrish 1981; Boulnois 1986). The total optical power on the sample is 1.5 mW, which avoids damage to biological tissue via thermal effects. Sensitivity of the OCT system defines the minimum detectable change in index of refraction and was experimentally measured as 91 dB. The theoretical axial resolution depends on the coherence length (l_c) of the OCT light source; interference fringes will occur if the optical path lengths of the reference and sample beams coincide within $\pm\, l_c$. Assuming a Gaussian spectrum, axial resolution is equal to $2\ln(2)\lambda^2/\Delta\lambda\pi n$, where λ is the center wavelength of the OCT beam, $\Delta\lambda$ is the spectral bandwidth (FWHM), and n is the refractive index of the sample medium (Fercher et al. 2003). The theoretical axial resolution of our OCT system is therefore 3.8 μm in air and 2.9 μm in water. In SDOCT, the design of the spectrometer and signal processing both affect the actual resolution. The spectrometer used in our OCT system can image a spectral range (δ) of 150 μm while the OCT software applies Hann-windowing of the spectrum to give smooth axial point-spread functions. The actual axial resolution of our system is $\lambda^2/(\delta n)$, equivalent to 5.8 μm in air and 4.3 μm in water. Lateral resolution is set by the minimum waist radius of the focused OCT beam, which in our system is 15 μm. The spectrometer used in our OCT system includes a 12 bit high-sensitivity CCD camera with 2.0 μm pixel spacing. Data are transferred in real-time over a GigE connection to a PC with a 3.3 GHz processor. The maximum scan rate of the OCT system used in this study is 29 kHz (equivalent to 56.6 fps for 512 A-lines per frame). The rate of data transfer and live streaming of the 2D OCT scan produce an actual recorded frame rate of 25.1 fps for a 512 A-line image (12.9 kHz). The sample refractive index is defined for the medium surrounding the sample and is considered 1.33 for both the microchannel and *in ovo* embryo imaging. A larger refractive index improves axial resolution as defined in the equation above. During imaging, all samples were positioned and mounted on a X–Y linear translation plus Z-axis rotation stage. This stage has accuracy of 25.4 μm per division to facilitate the velocity profiles measurement spanning across the width of the microchannel in the in vitro test.

2.4 μPIV algorithm

All synthetic and acquired OCT images were processed with DaVis 7.2 PIV software using a time-series sum of correlation calculation algorithm for steady flow

calculation and a time-series calculation algorithm for pulsatile flow calculation, which were also adopted from our previous studies (Patrick et al. 2011; Mikhail Lara et al. 2011; Chen et al. 2011). The first-pass PIV interrogation window was 32 × 32 pixel with 50 % overlap for 2 iterations, and the second-pass was 16 × 16 pixel interrogation size with 50 % overlap for 2 iterations. Multi-pass post-processing median filtering was used to remove neighboring bad vectors greater than 2 root mean square (R.M.S) and reinserted if less than 3 R.M.S. of neighboring vectors. A Probability Density Function analysis indicated that velocity values along the main flow direction were all less than 0.1-pixel which demonstrates the peak-locking effect (Chen and Katz 2005) was insignificant in all test cases. For the in vitro test, each depth-resolved velocity profile was calculated from 200 frames under a steady flow condition. This number was chosen since standard running-average convergence analysis (Lara et al. 2011) showed that the average velocity deviation at same interrogation window was on the order of 10^{-3} mm/s and the average velocity in the entire flow field was on the order of 10^{-1} mm/s. Minus two-order of velocity magnitude difference was found when more than 100 frames were processed.

2.5 Preparation of chick embryos

Fertilized White Leghorn chick eggs were incubated blunt end up at 37 °C and 50–60 % relative humidity to HH (Hamburger and Hamilton)-stage 18. Eggs were positioned under a stereomicroscope (M165FC, Leica Microsystems GmbH, Germany) and the embryos were exposed by windowing the shell and removing the overlying membranes. Embryos that were dysmorphic or exhibited overt bleeding were rejected (Kowalski et al. 2012; Wang et al. 2009).

3 Results and discussion

3.1 OCT-μPIV synthetic data

The main purpose of generating synthetic OCT-μPIV data sets is to investigate how the scan direction and speed affect the PIV calculated velocity results. When the scan directions were parallel to the main flow direction, the differences in scan speed (CCD capture and 33 fps) caused very minor velocity deviations as shown in the Fig. 1c. 1.03 mm/s of peak velocity was calculated using a standard whole-field acquisition method with a CCD camera (traditional PIV acquisition). The peak velocity was decreased slightly to be 1.01 mm/s when the 33 fps of scan speed and a scan direction, which was parallel to the main flow direction, were applied. In addition, 33 fps scan speed provided similar velocity profiles (almost overlapped with CCD capture results) with error arising only due to a slightly difference in the velocity peak region. This scan direction is believed to provide accurate velocity profiles as also evidenced by 80 fps results using the same scan mode (Fig. 1c).

On the contrary, when the scan direction was set to be perpendicular to the main flow direction, the effect of scan

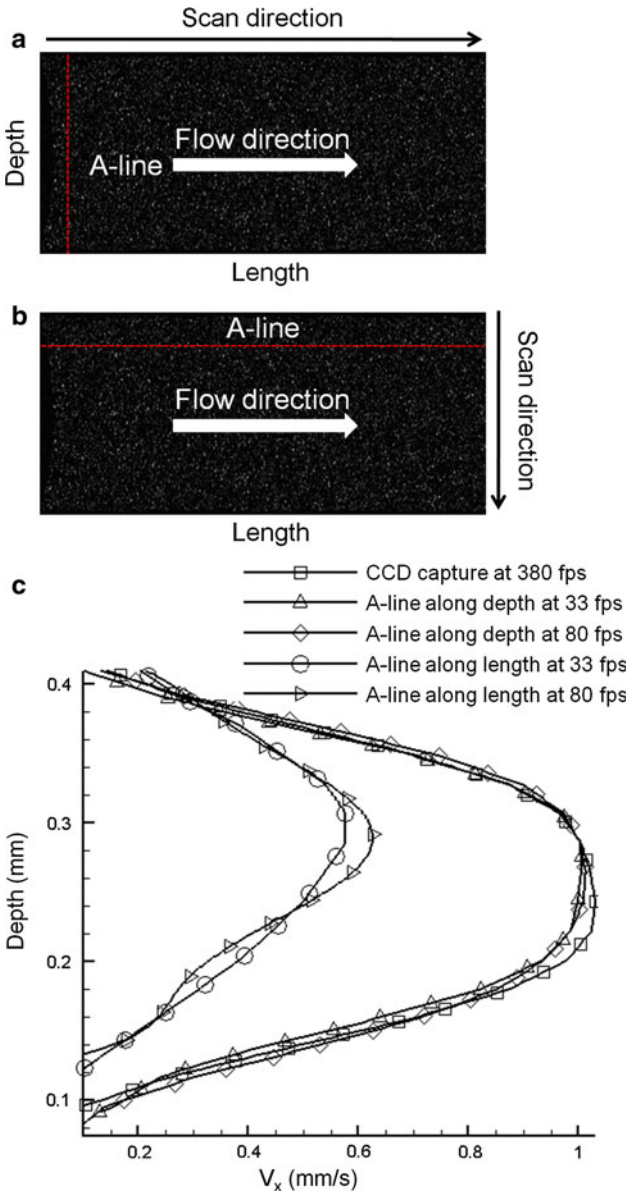

Fig. 1 Parametric analysis of OCT-μPIV technique using the *in-house* synthetic PIV data generator. Raw synthetic OCT-μPIV data: the two orthogonal scanning modes with the OCT-μPIV technique are illustrated. **a** Parallel to the flow direction; **b** Perpendicular to the flow direction. **c** These raw data were post-processed, and computed μPIV velocity profiles across the depth of the vessel are plotted under different scan directions and scan speeds. CCD capture corresponds to the traditional instantaneous whole-field PIV acquisition

speed became a dominant factor that affected velocity deviations significantly. In this case with a scan speed of 33 fps, the peak velocity reduced to be as low as 0.53 mm/s, which corresponds to ~49 % error compared to the whole-field CCD capture as also shown in Fig. 1c. In addition, under this scan direction, velocity profiles were skewed normal to the flow direction. Therefore, during in vitro and in vivo tests, it is recommended to have the scan direction parallel to the main flow to minimize these imaging artifacts.

3.2 In vitro validation test case

The tracer particle behavior and the capability of OCT-μPIV technique were further investigated in a real experimental setting, using a deep microchannel as the first validation case. The main purpose of this test is to show the accuracy of this technique in a typical micro-scale flow regime with known analytical solution. Specifically, it was used to check if our μPIV algorithm can resolve the time-dependent particle movement recorded by the OCT imaging system. A typical raw OCT image of the particle flow in the microchannel is provided in Fig. 2a (For further raw PIV data, please see "Appendix"). It is worth noting that by taking the depth sectioning capability of the OCT system, the acquired velocity profiles correspond to the particle distribution spanning from the top wall to the bottom wall, which enables the unique depth-resolved field of view (parallel to the sagittal plane). Unless special micro-fabrication and optical arrangements performed, this field of view is published first-time in the literature to our knowledge. The combination of depth-resolved and width-resolved flow data can be further used to generate a 3D velocity volumetric view of the entire flow domain utilizing interpolation routines (Frakes et al. 2008).

Representative processed μPIV results obtained from raw OCT images are shown in Fig. 2b as a velocity contour plot. Measured velocity distribution matches the prediction where the velocity profile is parabolic across the depth of the rectangular channel with peak value appearing along the centerline. Further quantitative comparison between the calculated OCT-μPIV data and theoretical solutions (Lima et al. 2006) at different flow rates and at different lateral positions are shown in Figs. 2c and 3. In Fig. 2c, calculated OCT-μPIV velocity values also agreed well with analytical solutions in a flow regime similar to microcirculation flow conditions in vertebrate such as chick (Lee et al. 2007) and zebrafish embryos (Chen et al. 2011) where the peak velocity in these animals is ranging from 1 to 3 mm/s. The accuracy achieved during this in vitro validation experiment encouraged our group to employ this technique in a more challenging in vivo experiment to study hemodynamics in embryos at early stages.

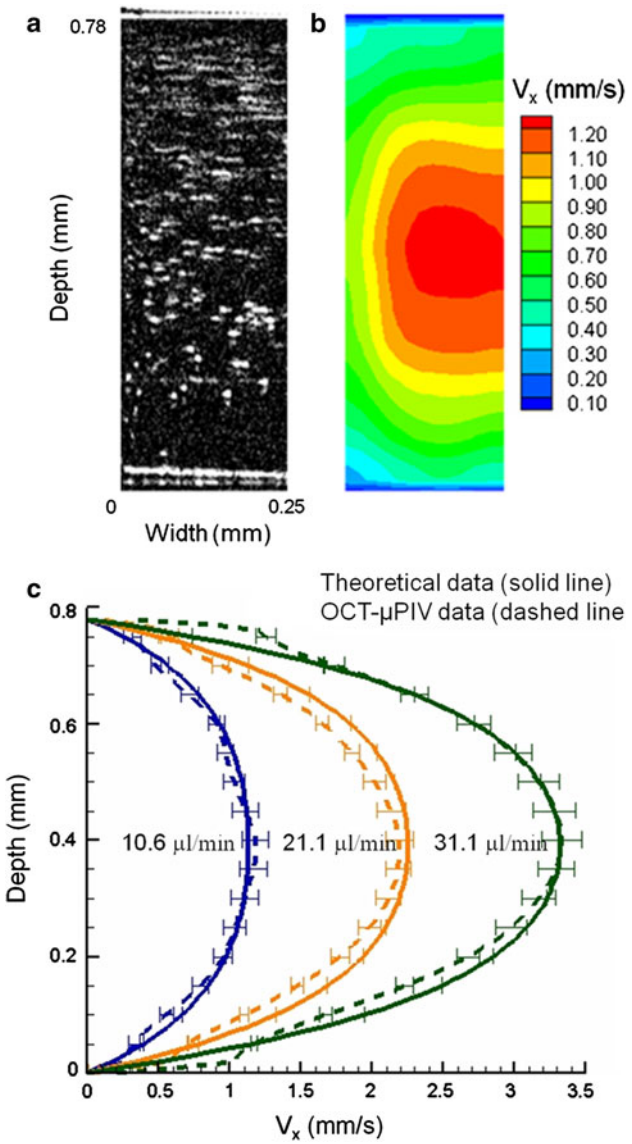

Fig. 2 **a** A snap shot of a depth-resolved raw OCT image of a 3.2-μm fluorescent particle flow in the microchannel. **b** Post-processed particle velocity contour plot using the OCT-μPIV algorithm from acquired raw OCT images. **c** Depth-resolved velocity profiles acquired at the center of the microchannel with three different flow rates compared with the corresponding analytical solutions. *Error bars* indicate one standard deviation values for each flow rate

3.3 In vivo flow acquisition in arterial blood vessels of early chick embryos

The velocity profile in a major extra-embryonic vitelline artery of chick embryo was studied (Fig. 4a) as an in vivo micro-scale test case. This vessel is particularly suitable to demonstrate the in vivo applicability of the present OCT-μPIV technique as its flow velocity and pulsatility had already been also documented in previous studies (Hu and Clark 1989; Lee et al. 2007; Poelma et al. 2008) using different measurement techniques. At embryonic

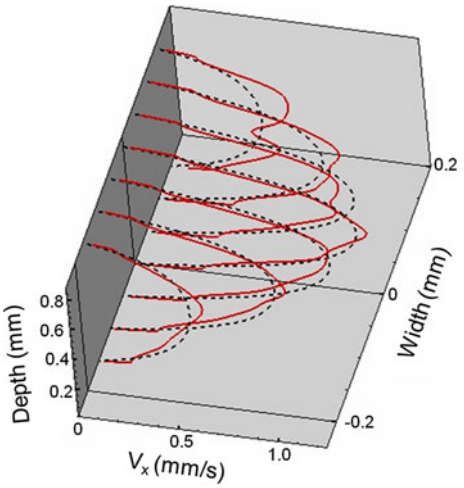

Fig. 3 Depth-resolved velocity profiles comparison between the OCT-μPIV calculated velocity profiles (*red solid lines*) and corresponding theoretical solutions (*dashed lines*) across the width of the microchannels. Seven planes were measured with a translational stage (25.4 μm per division) and compared which located at width = 0 (along centerline of the microchannel), ± 50.8, ± 101.6, ± 152.4 μm, respectively

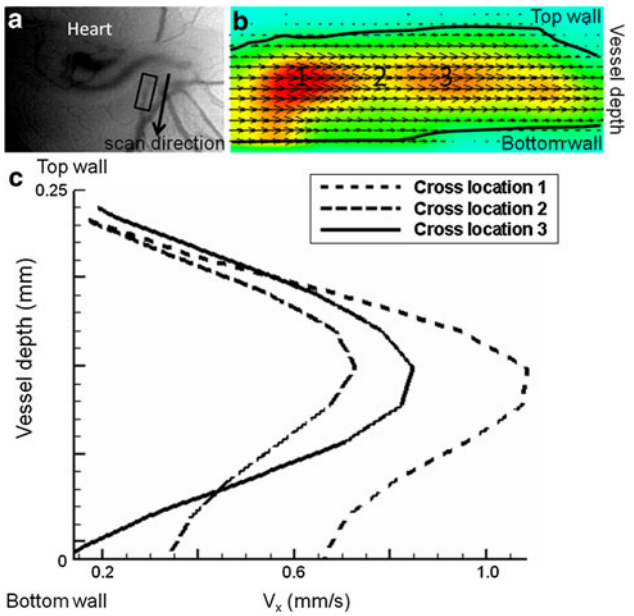

Fig. 4 Quantification of an in vivo arterial blood flow using OCT-μPIV along the middle sagittal plane spanning the vessel. **a** A selected scan location is outlined with black solid lines of the OCT beam across the depth of an vitelline artery in a HH (Hamburger and Hamilton)-stage 18 chick embryo. **b** Calculated depth-resolved velocity field using the OCT-μPIV algorithm. **c** Reconstructed velocity profile from the top to the bottom of the vessel walls across location 1, 2, and 3

stages (Stage 18–21, Hamburger-Hamilton), the vitelline artery is approximately 0.1–0.5 mm in diameter, highly variable in its cross-section (Wang et al. 2009; Kowalski et al. 2012). The measured axial blood flow field, at the mid-sagittal vessel plane using OCT-μPIV is plotted in Fig. 4b. The corresponding velocity profiles across the vessel depth were plotted across three locations 1, 2, and 3 in Fig. 4c. Despite the close proximity of our measurement location to the vessel bifurcation, approximately, parabolic depth-resolved velocity profiles (R-squared value = 0.99) were observed which validates the fully-developed flow assumption for the extra-embryonic circulation in the chick embryo. In addition, the peak velocity value along the vessel axis was variable as expected due to the variations in vessel cross-sectional area. The average peak velocity values measured by the OCT-μPIV was 1.1 mm/s which is very close to a reported value of ~1.5 mm/s from a previous studies (Lee et al. 2007) (exact match of velocity values are not possible since exact measurement locations are not provided). Reynolds number for this vessel was calculated to be on the order of 10^{-1}.

While the in vivo application of this new technique was demonstrated at a relatively straight vessel section, OCT-μPIV is expected to be very practical for studying flow fields where the flow structures can be more complex since the velocity profile can be sectioned at any angle. For example, when chick embryo arterial and venous vessels ran parallel (Fig. 5), OCT-μPIV can provide both velocity fields simultaneously without the need for special velocity encoding for each velocity range (from 0.1 to 3 mm/s). Furthermore, OCT-μPIV technique is particularly advantageous in studies that correlate flow-induced wall shear stress with vessel growth, as it can simultaneously provide vessel cross-section data and velocity information. Combining simultaneous anatomy (with a series of image processing methods such as thresholding, edge detection, and segmentation to track vessel wall precisely) and flow information in microchannels is a significant advantage of the OCT-μPIV technique as proposed in the present manuscript.

The OCT-μPIV technique is further capable of quantifying in vivo pulsatile blood flows. In order to achieve adequate temporal resolution in pulsatile blood flow conditions, the time-series μPIV algorithm was used. Time-dependent velocity values were sampled from two locations (at location 1 and 3 of Fig. 4b). The Power Spectrum Density (PSD) of the velocity signal result showed a consistent peak at 2.13 Hz corresponding to the heart rate of the embryo. This value was comparable with our CCD camera recordings as well as to the previous reported values which are 2.43 Hz (Hu and Clark 1989) and 1.95 Hz (Lee et al. 2007) for embryos at HH-stage 18. Given that the heart rate is highly dependent on the body temperature, this level of agreement is acceptable to demonstrate the capability of OCT-μPIV in in vivo pulsatile flows. Furthermore, the Womersley number is less than unity and the peak WSS in the arterial vessel was calculated to 0.02 Pa.

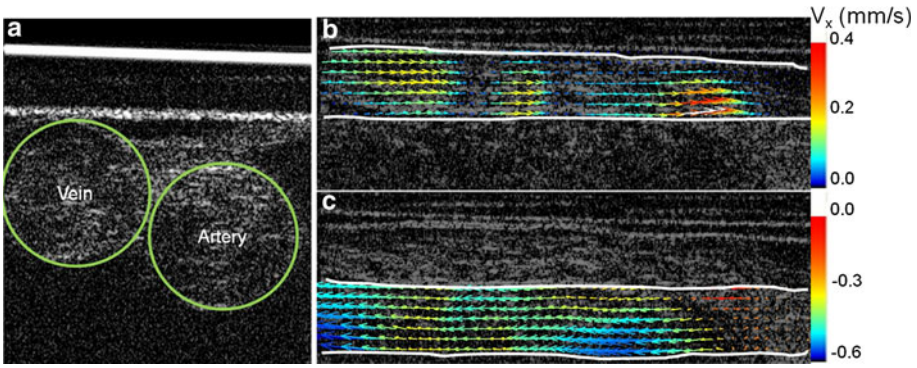

Fig. 5 Simultaneous flow assessment of arterial and venous blood vessels in chick embryos using OCT-μPIV. **a** A transverse view of both vessels. Calculated depth-resolved velocity fields in the venous vessel **b** and arterial vessel (**c**). Vessel boundary is outlined with *green* (**a**) and white (**b** and **c**) *sold lines*. The diameter of both vessels: 0.16 mm

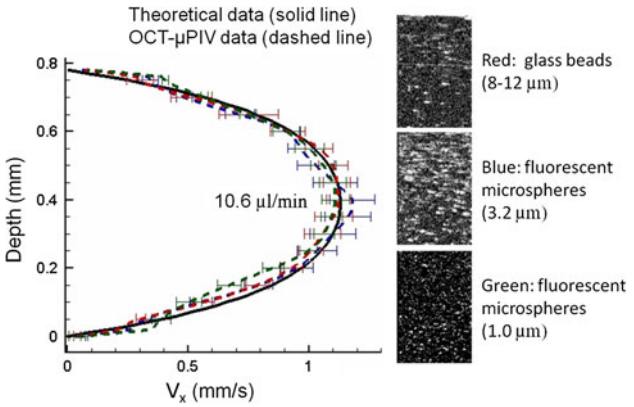

Fig. 6 Depth-resolved velocity profiles acquired at the center of the microchannel with three different types of particles compared with the corresponding analytical solutions. *Error bars* indicate one standard deviation values for each particle type. *Red*: hollow glass beads with 8–12 μm in diameter (TSI, Inc., MN) at concentration of 0.6 % (mg/mL); *Blue*: fluorescent particles with 3.2 μm in diameter (Microgenics, Inc., CA) at concentration of 0.2 %; *Green*: fluorescent particles with 1.0 μm in diameter (Microgenics, Inc., CA) at concentration of 0.1 %

4 Conclusions

A new micro-scale flow quantification technique was proposed in this study by combining OCT and μPIV processing. Depth-resolved flow profiles of tracer particles were quantified with a high-degree of agreement achieved in comparison with the theoretical solutions. This method has been demonstrated to be useful for in vivo flow measurements by experiments quantifying the blood flow in an arterial blood vessel of chick embryos. Acquired data were consistent with the previous reported values, including pulsatile flow frequency as well as peak velocity of the blood flow. Further, to report quantitative error estimation of calculated peak velocity value, synthetic OCT-μPIV data were generated based on the designed experimental scan and flow conditions. Maximum peak velocity error of 1 % was found as a function of the scan direction and scan rate. In this study, synthetic data as well as in vitro and in vivo experimental data were utilized to report the accuracy of this new technique, and the potential applications have been discussed. OCT-μPIV allows for comprehensive cardiovascular flow assessment integrated simultaneously with 3D quantitative anatomical measurement capabilities to improve studies of pulsatile hemodynamics in embryos at early stages. It is expected that the proposed novel technique will better equip researchers to facilitate hemodynamic quantification in embryonic animal models for development biology studies as it provides accurate and real-time depth-resolved flow assessment on embryonic animal models and fills an important gap in quantitative microscopic velocimetry techniques.

Acknowledgments This work was supported by NSF CAREER 0954465 and ERC Consolidator Grants.

Appendix

In PIV, a significant portion of measurement error can be caused by the tracer particle size. This error have been well established for a standard μPIV experiment (Lindken et al. 2009) but needs to be quantified for the new OCT-μPIV technique. In order to investigate particle size effect on the OCT-μPIV velocity measurements, three different types of particles were tested that range from 1 to 12 μm. The resultant velocity profiles obtained with these particles were plotted in Fig. 6 along with corresponding analytical solution comparison and the raw OCT-μPIV images. Through this comparison, the optimal ratio of particle size to the relevant fluid dynamic length scale should be in the range of 0.03 (12/400 μm) and 0.003 (1/400 μm). In this work, the channel width was fabricated to be 400 μm, and therefore, the particle size of 3.2 μm was selected to ensure that the particle response time is smaller than the smallest time scale in the flow and free of Brownian motion effects. The calculated interparticular distance values for 12, 3.2, and 1.0 μm particles are 94, 38, and 16.7 μm, respectively.

References

Bogren HG, Buonocore MH, Valente RJ (2004) Four-dimensional magnetic resonance velocity mapping of blood flow patterns in the aorta in patients with atherosclerotic coronary artery disease compared to age-matched normal subjects. J Magn Reson Imaging 19(4):417–427

Boulnois J-L (1986) Photophysical processes in recent medical laser developments: a review. Lasers Med Sci 1:47–66

Brezinski ME (2006) Optical coherence tomography: principles and applications. Academic Press, London

Chen J, Katz J (2005) Elimination of peak-locking error in PIV analysis using the correlation mapping method. Meas Sci Technol 16(8):1605–1618

Chen C-Y, Patrick MJ, Corti P, Kowalski W, Roman BL, Pekkan K (2011) Analysis of early embryonic great-vessel microcirculation in zebrafish using high-speed confocal μPIV. Biorheology 48:305–321

Corti P, Young S, Chen CY, Patrick MJ, Rochon ER, Pekkan K, Roman BL (2011) Interaction between alk1 and blood flow in the development of arteriovenous malformations. Development 138(8):1573–1582

Davis A, Izatt J, Rothenberg F (2009) Quantitative measurement of blood flow dynamics in embryonic vasculature using spectral Doppler velocimetry. Anat Record (Hoboken) 292(3):311–319

Drexler W, Fujimoto JG (2008) Optical coherence tomography: technology and applications (biological and medical physics, biomedical engineering). Springer, Berlin

Fercher AF, Drexler W, Hitzenberger CK, Lasser T (2003) Optical coherence tomography—principles and applications. Rep Prog Phys 66:239–303

Frakes DH, Pekkan K, Dasi LP, Kitajima HD, de Zelicourt D, Leo HL, Carberry J, Sundareswaran K, Simon H, Yoganathan AP (2008) Modified control grid interpolation for the volumetric reconstruction of fluid flows. Exp Fluids 45(6):987–997

Hahn C, Schwartz MA (2009) Mechanotransduction in vascular physiology and atherogenesis. Nat Rev Mol Cell Biol 10(1): 53–62

Hove JR, Koster RW, Forouhar AS, Acevedo-Bolton G, Fraser SE, Gharib M (2003) Intracardiac fluid forces are an essential epigenetic factor for embryonic cardiogenesis. Nature 421(6919): 172–177

Hu N, Clark EB (1989) Hemodynamics of the stage 12 to stage 29 chick embryo. Circ Res 65(6):1665–1670

Huang D, Swanson EA, Lin CP, Schuman JS, Stinson WG, Chang W, Hee MR, Flotte T, Gregory K, Puliafito CA et al (1991) Optical coherence tomography. Science 254(5035):1178–1181

Kim GB, Lee SJ (2006) X-ray PIV measurements of blood flows without tracer particles. Exp Fluids 41(2):195–200

Kim HB, Hertzberg JR, Shandas R (2004) Development and validation of echo PIV. Exp Fluids 36(3):455–462

Kowalski WJ, Teslovich NC, Dur O, Keller BB, Pekkan K (2012) Computational hemodynamic optimization predicts dominant aortic arch selection is driven by embryonic outflow tract orientation in the chick embryo. Biomech Model Mechanobiol 11(7):1057–1073

Lara M, Chen CY, Mannor P, Dur O, Menon PG, Yoganathan AP, Pekkan K (2011) Hemodynamics of the hepatic venous three-vessel confluences using particle image velocimetry. Ann Biomed Eng 39(9):2398–2416

Lee JY, Ji HS, Lee SJ (2007) Micro-PIV measurements of blood flow in extraembryonic blood vessels of chicken embryos. Physiol Meas 28(10):1149–1162

Lima R, Wada S, Tsubota K, Yamaguchi T (2006) Confocal micro-PIV measurements of three-dimensional profiles of cell suspension flow in a square microchannel. Meas Sci Technol 17(4):797–808

Lindken R, Westerweel J, Wieneke B (2006) Stereoscopic micro particle image velocimetry. Exp Fluids 41(2):161–171

Lindken R, Rossi M, Grosse S, Westerweel J (2009) Micro-particle image velocimetry (microPIV): recent developments, applications, and guidelines. Lab Chip 9(17):2551–2567

Markl M, Harloff A, Bley TA, Zaitsev M, Jung B, Weigang E, Langer M, Hennig J, Frydrychowicz A (2007) Time-resolved 3D MR velocity mapping at 3T: improved navigator-gated assessment of vascular anatomy and blood flow. J Magn Reson Imaging 25(4): 824–831

Oosterbaan AM, Ursem NT, Struijk PC, Bosch JG, van der Steen AF, Steegers EA (2009) Doppler flow velocity waveforms in the embryonic chicken heart at developmental stages corresponding to 5–8 weeks of human gestation. Ultrasound Obstet Gynecol 33(6):638–644

Park JS, Kihm KD (2006) Three-dimensional micro-PTV using deconvolution microscopy. Exp Fluids 40(3):491–499

Park JS, Choi CK, Kihm KD (2004) Optically sliced micro-PIV using confocal laser scanning microscopy (CLSM). Exp Fluids 37(1): 105–119

Parrish JA (1981) New concepts in therapeutic photomedicine: photochemistry, optical targeting and the therapeutic window. J Investig Dermatol 1:45–50

Patrick MJ, Chen CY, Frakes D, Dur O, Pekkan K (2011) Cellular-level near-wall unsteadiness of high-hematocrit erythrocyte flow using confocal μPIV. Exp Fluids 50:887–904

Poelma C, Vennemann LindkenR, Westerweel J (2008) In vivo blood flow and wall shear stress measurements in the vitelline network. Exp Fluids 45(4):703–713

Roman BL, Pekkan K (2012) Mechanotransduction in embryonic vascular development. Biomech Model Mechanobiol

Srinivasan S, Baldwin HS, Aristizabal O, Kwee L, Labow M, Artman M, Turnbull DH (1998) Noninvasive, in utero imaging of mouse embryonic heart development with 40-MHz echocardiography. Circulation 98(9):912–918

Sundareswaran KS, Haggerty CM, de Zelicourt D, Dasi LP, Pekkan K, Frakes DH, Powell AJ, Kanter KR, Fogel MA, Yoganathan AP (2011) Visualization of flow structures in Fontan patients using 3-dimensional phase contrast magnetic resonance imaging. J Thorac Cardiovasc Surg 143(5):1108–1116

Wang Y, Dur O, Patrick MJ, Tinney JP, Tobita K, Keller BB, Pekkan K (2009) Aortic arch morphogenesis and flow modeling in the chick embryo. Ann Biomed Eng 37(6):1069–1081

Weinbaum S, Tarbell JM, Damiano ER (2007) The structure and function of the endothelial glycocalyx layer. Annu Rev Biomed Eng 9:121–167

Weissmann-Brenner A, Pretorius DH, Achiron R, Gindes L (2012) Fetal echocardiography: the four-chamber view, the outflow tracts, and the contribution of the cardiac arches. Ultrasound Clin 7(1):1–13

Zheng H, Liu L, Williams L, Hertzberg R, Lanning C, Shandas R (2006) Real time multicomponent echo particle image velocimetry technique for opaque flow imaging. Appl Phys Lett 88(26):261915